Brojomohun College, Barisal

Subject Name

THESIS ON
Calcium Manganese Titanium Oxide (CaMnTiO3)

Supervised By

Teacher Name
Lecturer
Faculty of Faculty Name
Brojomohun College, Barisal

Submitted By

Your Name

ID: XXXXXXXXXXXX

Publish Year **2016-2017**
26 October, 2016

Declaration

This is to certify that this project is our original work. No part of this has been submitted elsewhere partially or fully for the award of any other degree. Any material reproduced in this project has been properly acknowledged.

_____

Name: Your Name

ID: XXXXXXXXXXX

Approval

The Thesis titled "Calcium Manganese Titanium Oxide" has been submitted to the following respected members of the Board of Examiners of <u>Faculty Name</u> in complete fulfillment of the requirements for the department of <u>department name</u> and engineering on <u>Date</u> by the following student and has been accepted satisfactory.

_____

Teacher Name
Lecturer
Department of <u>Department Name</u>
<u>College Name</u>

_____

Teacher Name
Head of the Department
Department <u>Department Name</u>
<u>College Name</u>

_____

Teacher Name
Dean in Charge
Department of <u>Department Name</u>
<u>College Name</u>

_____

Teacher Name
Vice Chancellor
Department of <u>Department Name</u>
<u>College Name</u>

Acknowledgements

We would like to take the chance to express our gratitude to our honorable teacher & Supervisor Teacher Name, for his continuous guidance and support regarding this report. Besides this, I have found so many sincere and productive advices from many people that we would like pay homage to them.

Table of Contents

SURFACE COMPOSITION AND CHEMICAL STATES OF CALCIUM MANGANITES

ABSTRUCT

This paper describes investigations on atomic composition and chemical states of sintered calcium manganites discs in surface and near surface regions. The atomic composition was determined by 3.05 $MeV^{16}O(\alpha,\alpha)^{16}O$ resonance elastic scattering while the chemical states by, X-ray photoelectron spectroscopy (XPS). The specimens examined included undoped and donor (Y^{3+}, Bi^{3+}) doped $CaMnO_3$, and Ca-excess and Mn-excess manganites namely Ca_2MnO_4 and $CaMn_2O_4$ respectively. Calcium manganite powder used in the preparation of discs was synthesized by a wet chemical method. X-ray diffraction (XRD) results indicated that all the discs are monophasic except $CaMn_2O_4$, which contained ~98% requisite manganite.

The atomic compositions of undoped specimens are close to the stoichiometric value while Y^{3+} and Bi^{3+} doped specimens are deficient in Mn and O respectively. The O deficiency may be responsible for comparatively higher electrical conductivity of Bi^{3+} doped specimen. Some of the specimens were also examined subsequent to their annealing in low PO_2 atmosphere.

This treatment produced significant compositional and structural modifications in the near surface regions. Mn(2p) electrons have identical binding energies in the sintered discs; therefore the valence states of Mn could not be discerned. However lesser binding energies of these electrons in annealed $CaMnO_3$ indicated the existence of Mn(II)/Mn(III) in the specimen.

1.1 INTRODUCTION

Manganites with perovskite structure exhibit several interesting electronic and magnetic phenomena such as insulator-metal transition and colossal magnetoresistance (CMR). Consequently, these materials have been intensively studied in recent years. These oxides can be represented by a general formula $Ln_{1-x}A_xMnO_3$ with Ln being a rare earth element and A, an alkaline earth element.

The properties of materials depend on the content of x, nature and extent of doping and processing parameters. CaMnO3, the basic unit of these perovskites, is itself of great interest. It is an n-type semiconducting oxide and exhibits anti ferromagnetic ordering at TN < 130 K as well. Incorporation of dopants introduces significant changes in the electrical properties of the material. It can also be electron doped by annealing in lower PO2 atmosphere to produce oxygen deficient nonstoichiometric perovskite, $CaMnO_{3-\delta}$. The electrical and magnetic properties of $CaMnO_{3-\delta}$ are influenced by oxygen content as well as the valence states of manganese.

Surface characterization of manganites is important in fabricating multilayer thin film devices that make use of the CMR properties. In the present work we have studied the atomic composition, in the near surface regions, of sintered discs of undoped and donor (3 at% Bi^{3+} and Y^{3+}) doped $CaMnO_3$ as well as Ca-excess and Mn-excess manganites namely Ca_2MnO_4 and $CaMn_2O_4$ respectively by 3.05 MeV $^{16}O(\alpha,\alpha)^{16}O$ elastic resonance scattering.

Some of the specimens were also examined subsequent to their annealing in hydrogen atmosphere to study the compositional and structural variations accompanying the reduction process. This resonance scattering with significantly higher cross section is a well established backscattering spectrometry technique for depth profiling oxygen in the near surface regions non-destructively. It has been used in the analysis of several oxide matrices including Y–Ba–Cu–O superconductors.

However such a study on manganites is lacking as most analytical studies deal with the determination of oxygen by classical chemical methods. The estimated composition has been discussed in correlation with structural and phase analysis of the ceramics by XRD. In addition, we have also investigated the chemical states of manganese in these oxides by XPS.

1.2 SAMPLE PREPARATION

Polycrystalline samples of calcium manganite were synthesized by a wet chemical method involving a redox reaction between Mn(VII) and Mn(II) salts in nitric acid medium the details of which are reported in a previous publication. Briefly concentrated HNO3 was added to aqueous solution of KMnO4 to maintain the pH in 1–2 range and heated to boiling conditions.

The homogeneous solution of Ca(NO3)2 . 4H2O and MnSO4 . H2O, mixed in the desired ratio, was added to the boiling KMnO4 solution to precipitate MnO2 Æ xH2O. Due to its larger porosity and high surface area, the precipitated MnO2 · xH2O adsorbed other cations. The pH was raised to 7 by adding 2 M ammonium carbonate to complete the precipitation of the metal cations.

The precipitate was filtered and washed with deionised water for complete removal of anions such as Cl- and SO_4^{2-} and subsequently oven dried at 373 K. The dry powder was decomposed at 850 K followed by calcination at 1373 K for 5 h. The powder of calcium manganite thus obtained was mixed with 0.1 wt.% polyvinyl alcohol, a binder, and then pressed into pellets (thickness, 2 mm; diameter, 10 mm) in a hydraulic press at 200 MPa and subsequently sintered in air at 1573K for 3h. Specimens doped with 3at% Bi^{3+} and Y^{3+} were prepared by intimately mixing the oxides of Y and Bi in the requisite proportions with calcium manganite powder and calcining at 1000 K for 3h.

The doped powder was then pelletised and sintered as described earlier. Some of the sintered specimens were annealed in N2 + H2 (1:1) atmosphere at 1373 K for 2 h to produce O deficient manganites.

1.3 BACKSCATTERING SPECTROSCOPY (BS) MEASUREMENTS

The BS measurements were carried out using 3MV Tandetron at National Centre for Compositional Characterisation of Materials (NCCCM), Hyderabad. The a particle beam (/ = 1.5 mm) of requisite energy impinged on the targets at normal incidence in a typical scattering chamber.

The vacuum in scattering chamber, pumped by a turbomolecular pump, was about $2 \cdot 10\_6$ Torr. An electron suppressor with _900 V was placed in front of the samples. The particles scattered at 170_ were measured with a surface barrier detector and the data acquired on a PC based multichannel analyser.

1.4 DETERMINATION OF ATOMIC COMPOSITION

The $^{16}O(\alpha,\alpha)^{16}O$ resonant scattering occurs at the surface when the target is bombarded with 3.05 MeV α particles. It occurs from deeper layers of the target at higher incident energies. Therefore the depth profiling of O is accomplished by increasing the incident beam energy beyond 3.05 MeV in steps.

The relative atomic composition of $CaMn_pO_q$ by this method can be estimated by using the formula: $q = R \times [\epsilon(Ca) + p\epsilon(Mn)]/[\epsilon(Si)/2 + 1 - R \times \epsilon(O)]$ where ϵ is the stopping cross section of the elements in the brackets, R is the ratio of resonant O yields for $CaMn_pO_q$ and a 3000 A ° SiO_2 film, used as a standard for oxygen. The quantity p was determined from the BS spectrum by taking the signals of Ca and Mn into consideration.

It is noted that their scattering cross sections are Rutherford in the beam energy region used in the experiments. The depth scale was established by the relation $(E\alpha - Er)/S(E)$ where $E\alpha$ is the energy of the incident beam, Er is the resonance energy and S(E) is the stopping power at Er. The stopping cross sections and powers were computed by SRIM 2000. The density of the discs required for computing S(E) was estimated by geometrical methods.

1.5 XPS AND XRD MEASUREMENTS

The XPS measurements were performed with VG-Scientific ESCALAB Mk200X machine, using AlKα X-rays in a vacuum of 2×10^{-9} Torr. The energy scale of the spectrometer was calibrated with pure Ag and Cu samples. The binding energies were measured with a precision of ± 0.25 eV.

The XRD measurements for identifying crystalline phases in the ceramics were carried out by a Scintag (USA) diffractometer with CuKα radiation.

1.5 RESULTS AND DISCUSSION

The specimens are well sintered to more than 95% of theoretical density. XRD results indicate the sintered discs of CaMnO3, undoped as well as doped with 3at% Y^{3+} and Bi^{3+}, are monophasic with perovskite structure and orthorhombic symmetry of space group Pbma. The disc of Ca_2MnO_4 is also phase singular having K_2NiF_4 type structure while that of $CaMn_2O_4$ contains ~98% of the desired manganite, with marokite structure together with the minor phase of $CaMnO_3$. The annealing of $CaMnO_3$ and $CaMn_2O_4$ in hydrogen atmosphere resulted in the formation of defect rock salt $CaMnO_2$, and $CaMnO_{2.5}$ of brownmillerite type structure, respectively. The different phases present in sintered and annealed specimens along with their crystal symmetries are given in **Table 1.**

Table 1
Phases, crystal symmetries and resistivities of calcium manganites at 293 K

Composition	Phase contents	Crystal symmetry	Resistivity (Ω cm)
$CaMnO_3$	Perovskite	Orthorhombic	0.84
$CaMnO_3$ (3 at% Y^{3+})	Perovskite	Orthorhombic	0.12
$CaMnO_3$ (3 at% Bi^{3+})	Perovskite	Orthorhombic	0.06
Ca_2MnO_4	K_2NiF_4 type structure	Tetragonal	–
$CaMn_2O_4$	98.5% Marokite 1.5% Perovskite	Orthorhombic Cubic	8×10^3
$CaMnO_3$[a]	Rock salt ($CaMnO_2$)	Cubic	–
$CaMn_2O_4$[b]	Brownmillerite ($CaMnO_{2.5}$)	Cubic	–
$CaMn_2O_4$[c]	88% Marokite 12% Perovskite	Orthorhombic Cubic	–

(–): Not measured.
[a] $CaMnO_3$ annealed in $N_2 + H_2$ (1:1) atmosphere at 1373 K for 3 h.
[b] $CaMn_2O_4$ annealed in $N_2 + H_2$ (1:1) atmosphere at 1373 K for 3 h (top portion).
[c] $CaMn_2O_4$ annealed in $N_2 + H_2$ (1:1) atmosphere at 1373 K for 3 h (cleaved portion).
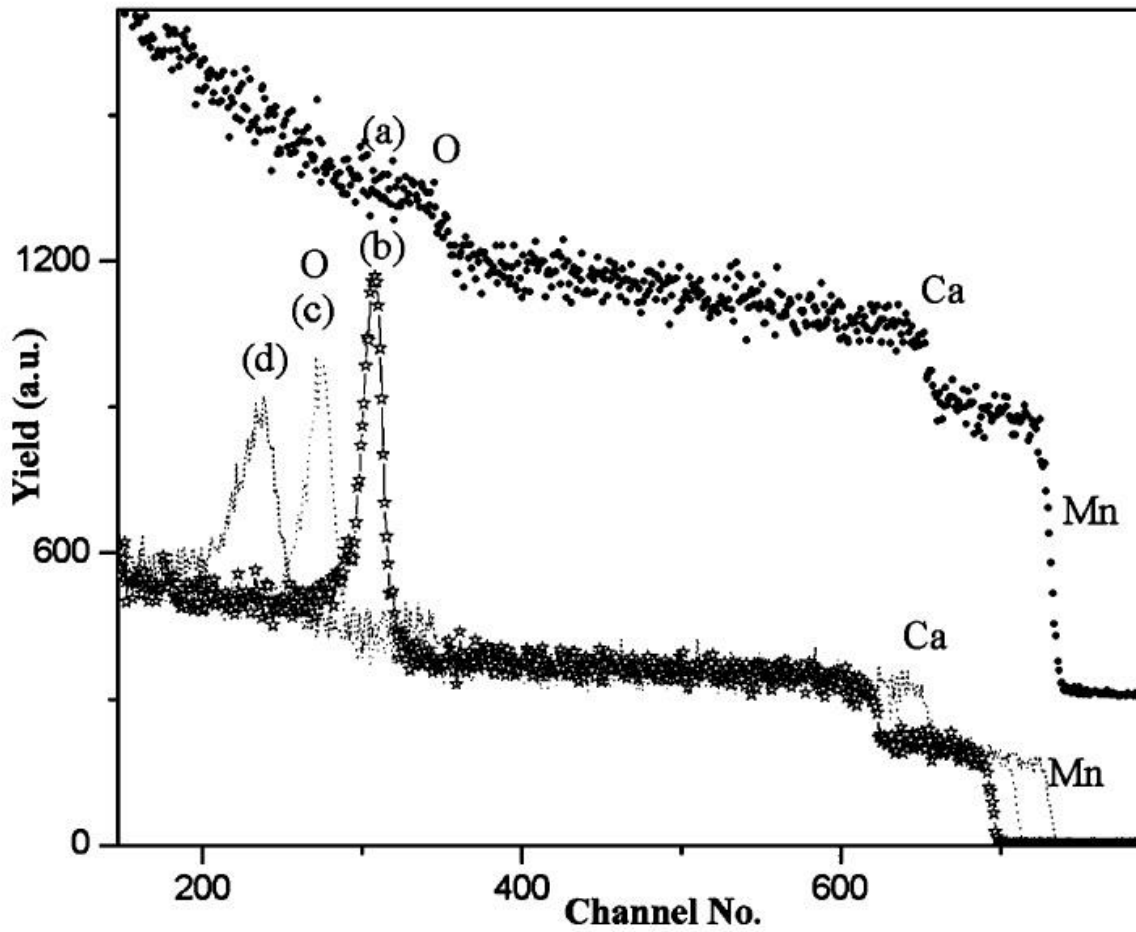
Figure 1.5.1: MeV α-RBS spectrum form CaMnO3 and (b), (c)
and (d) depth profile of oxygen in CaMnO$_3$ obtained with 3.07,
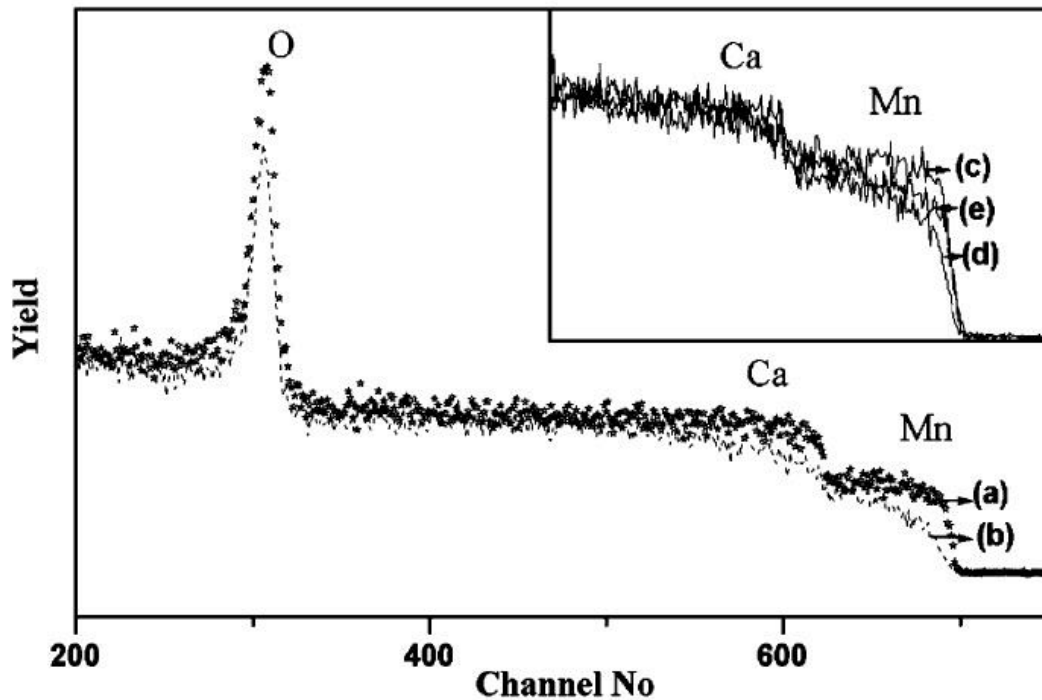3.13 and 3.23 MeV α particles respectively.

Figure 1.5.2: MeV α-backscattered spectra from (a) sintered

CaMnO3 and (b) after annealing it in hydrogen atmosphere.

Inset shows the leading edges of Mn and Ca from (c) sintered

CaMn$_2$O$_4$ (d) after annealing in hydrogen and (e) cracked

interior surface of the annealed specimen.

Figure 1.5.1(b)–(d) shows backscattered spectra from an undoped sintered CaMnO$_3$ specimen recorded with 3.07, 3.13 and 3.23 MeV a particles for depth profile measurements of oxygen. The occurrence of oxygen signal as a strong peak is due to $^{16}O(\alpha,\alpha)^{16}O$ resonant scattering. This approach is clearly advantageous over conventional RBS where the oxygen signal, as shown in Fig. 1.5.1(a), appears a weak step over the signals of Ca and Mn. The oxygen signal in Fig. 1(b)-

d) is a measure of its content at a depth of about 600 A ˚ , 2500 A ˚ and 5300 A ˚ respectively. The height of oxygen signal decreases while its width increases with beam energy due to straggling effects but the area under the signal is constant for a homogeneous target.

Fig. 1.5.2(a) is the backscattered spectrum for an undoped sintered CaMnO3 while Fig. 2(b) is from the same specimen annealed in hydrogen atmosphere. These spectra are normalized with respect to charge. It can be readily seen that in comparison to the sintered specimen, the annealed specimen has two significantly different spectral features: (1) the oxygen signal intensity is diminished and (2) the slopes of the leading edges of cations, Mn in particular, are less. These features are indicative of surface modifications resulting from annealing with the decrease in oxygen signal intensity signifying, expectedly, the reduction of the specimen. The second feature showing the depletion of Ca and Mn in the near surface regions is, however, interesting. The reduced specimen of $CaMn_2O_4$ also exhibits similar spectral features. The 3.07 MeVα backscattered spectra from this manganite and its annealed form are shown in Fig. 1.5.2(c) and (d) respectively for illustration. The specimen had in fact cracked horizontally into two parts during annealing. The spectrum in Fig. 1.5.2(d) is from the top part of the cracked sample. The underlying part was also examined along the surface exposed due to cracking and the resulting spectrum is shown in Fig. 1.5.2(e). It is observed by comparing the spectra in Fig. 1.5.2(c)-(e) that the slopes of the leading edges of Ca and Mn for the bottom part are more than those of the corresponding top part of annealed disc but still less than the sintered specimen. This can be attributed to the mild reduction of the specimen with crack facilitating the process. It is supported by the fact that the bottom part contains marokite as the major phase (88%) while the top part as mentioned earlier, contains only brownmillerite phase. It suggests that the interiors of the samples were not affected by annealing. The atomic composition of different specimens as a function of depth determined by 3.05 MeV $^{16}O(\alpha,\alpha)^{16}O$ resonant scattering is listed in Table 1. The errors in the estimation of atomic ratio of Ca to Mn and depth profiles of oxygen are about 3% and 6% respectively. These are however higher in the case of reduced specimens due to rapidly varying signal intensities. The estimated compositions of the undoped $CaMnO_3$ and Ca_2MnO_4 are in agreement with their respective nominal stoichiometries. The Y^{3+} doped $CaMnO_3$ specimen is deficient in Mn while the one doped with Bi^{3+}, in oxygen. It is to be noted that the oxygen content in the Bi^{3+} doped specimen is marginally less that the error associated with its measurement. Nevertheless in view of the

constancy of the value for repeated measurements, one at even higher depth, it can be surmised that the specimen is depleted in oxygen in comparison to undoped or Y^{3+} doped $CaMnO_3$. $CaMn_2O_4$ is enriched with Mn while oxygen stabilizes to its stoichiometric value at a depth of about 2000 A ° . The excess of oxygen in surface regions may be due to adsorbed oxygen bearing species. In the case of annealed specimens, it is evident that reduction in hydrogen atmosphere causes considerable alteration in the composition with the relative contents of Mn and O decreasing significantly, particularly in the case of $CaMn_2O_4$. Further, the atomic composition of the bottom portion of the cracked specimen of $CaMn_2O_4$ is nearly identical to that of sintered $CaMn_2O_4$ due to its reduction to a lesser extent. It is in agreement with the conclusions drawn from the qualitative spectral analysis.

The reduction of $CaMnO_3$ and $CaMn_2O_4$ to $CaMnO_2$ and $CaMnO_{2.5}$ respectively involves loss of oxygen according to the following reactions:
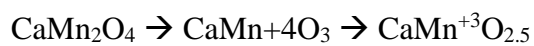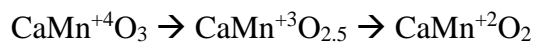
$CaMn^{+4}O_3$ → $CaMn^{+3}O_{2.5}$ → $CaMn^{+2}O_2$
$CaMn_2O_4$ → $CaMn+4O_3$ → $CaMn^{+3}O_{2.5}$

The phase singularity of annealed $CaMnO_3$ is in agreement with the above formalism. However, the conformity observed between the compositional and phase analyses of sintered specimens is The phase singularity of annealed $CaMnO_3$ is in agreement with the above formalism. However, the conformity observed between the compositional and phase analyses of sintered specimens is lacking, as there is a significant gradient in the concentration of oxygen in the surface regions. Furthermore, the depletion of Ca and Mn in identical concentrations maintains the relative atomic ratio of Ca and Mn close to unity. The surface depletion of Mn on reduction is distinctly observed in the case of $CaMn_2O_4$. So far as its reduction formalism is concerned, the formation of $CaMnO_3$ in the first step of the reaction is confirmed by increase in the content of CaMnO3 phase from 1.5% in the sintered $CaMn_2O_4$ to 12% in the mildly reduced bottom portion of the cracked specimen. Calcium manganites thus formed are obviously accompanied by manganese oxides that are often non-stoichiometric. It is to be noted that depletion of Mn does not imply its loss, as manganese oxides are nonvolatile even at higher temperatures. Under this consideration, the present

observation can be ascribed to either precipitation and or migration of Mn bearing species during the reduction process, which escape detection, by XRD and BS. The non-stoichometric phases formed often lack sufficiently large crystalline domains and therefore may not be identified by conventional structure determination technique.
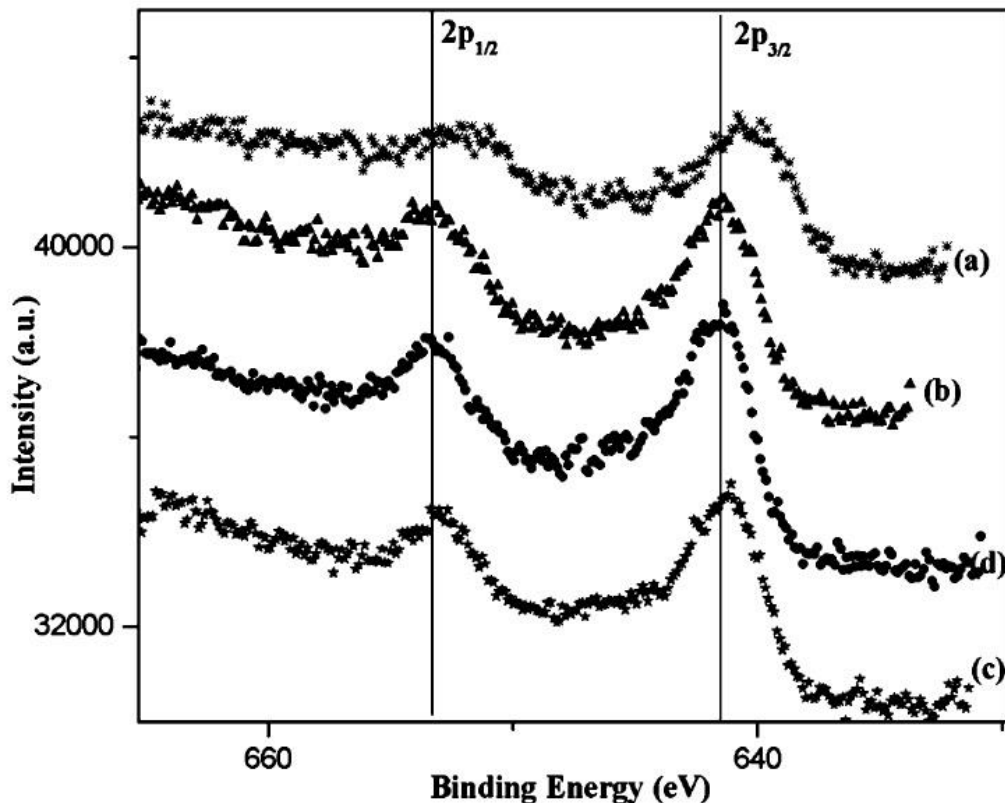

Figure 1.5.3: Mn(2p) electron spectra of (a) CaMnO$_3$ (reduced), (b) CaMn2O4 (sintered), (c) CaMn$_2$O$_4$ (reduced, top portion) and (d) CaMn$_2$O$_4$ (reduced, cracked portion).

The specimens were analysed by core level XPS to obtain information on the chemical states of the constituents. Fig. 1.5.3 shows the Mn(2p) electron spectra of different specimens. The spectra exhibit 2p1/2 and 2p3/2 spin–orbit doublets. The Mn(2p) peaks, in agreement with previous

studies, are broad and asymmetrical towards high binding energy side. Abbate et al. have explained

the reasons for the larger breadth of the peaks.

Table 2
Atomic composition of calcium manganite specimens in near surface regions

Sample	Depth (Å)	Atomic composition $(N_{Ca}:N_{Mn}:N_O)$
$CaMnO_3$	600	1.0:1.0:3.1
	2500	1.0:1.0:3.1
$CaMnO_3{}^a$	600	1.0:0.9:1.5
	1700	1.0:0.9:2.2
	2500	1.0:0.8:2.4
$CaMnO_3$ (3 at% Y^{3+} doped)	600	1.0:0.9:3.2
	2500	1.0:0.9:3.1
$CaMnO_3$ (3 at% Bi^{3+} doped)	600	1.0:1.0:2.8
	2500	1.0:1.0:2.8
	5100	1.0:1.0:2.8
$CaMn_2O_4$	800	1.0:2.2:4.4
	2800	1.0:2.2:4.1
	3800	1.0:2.2:4.2
$CaMn_2O_4{}^b$	800	1.0:1.2:2.0
	2800	1.0:1.2:1.9
	3800	1.0:1.1:1.6
$CaMn_2O_4{}^c$	800	1.0:2.0:3.8
	1900	1.0:2.1:3.9
	3800	1.0:2.0:4.1

[a] $CaMnO_3$ annealed in $N_2 + H_2$ (1:1) atmosphere at 1373 K for 3 h.
[b] $CaMn_2O_4$ annealed in $N_2 + H_2$ (1:1) atmosphere at 1373 K for 3 h (top portion).
[c] $CaMn_2O_4$ annealed in $N_2 + H_2$ (1:1) atmosphere at 1373 K for 3 h (cracked bottom portion).

Oku et al. have measured the binding energies of Mn(2p3/2) electrons in different manganese

oxides. These are also listed in Table 2. It can be seen that the chemical shift is appreciable only

in MnO and MnO2. The study also concluded neither the two oxidation states of Mn in Mn3O4

nor Mn site differences in Mn2O3 are distinguishable by XPS. In previous XPS studies on CaMnO3 and several $CaMnO_{3-\delta}$ compounds with different d values, the binding energy of Mn 2p3/2 electrons was reported to be identical (641.9 eV) in each compound. However in the present studies, it is about 641.7 eV in all the specimens except annealed CaMnO3 where it is about 640.6 eV. It is to be noted that the surfaces of reduced specimens were distinctly green providing indication of existence of Mn in +3 valence states. The higher binding energy of Mn 2p3/2 electrons in air sintered CaMnO3 suggests Mn to be in +4 valence state, occupying sites with octahedral O coordination.

The reduction of CaMnO3 involves introduction of O vacancies and conversion of Mn4+ ions into lower oxidation states. The lower binding energy in $CaMnO_{3-\delta}$ is indicative of this process. The differences in the binding energies in $CaMnO_{3-\delta}$ in the present study and may be due to different conditions of reduction. MnO and CaO also have rocksalt structure. The lower binding energies of Mn (2p) electrons in such samples eliminate the possibility of formation of MnO, which due to its pyrophoric nature, gets converted to Mn3O4. Similarly CaO reacts with atmospheric CO2, to produce CaCO3. The C (1s) electron spectra of each specimen showed only one peak corresponding to the adventitious carbon. The absence of a peak in 287–289 eV in the C (1s) spectra, characteristic of CO_3^{2-} , is therefore indicative of the absence of CaO as well.

The binding energies of Ca(2p) electrons in the specimens are also nearly identical. The slight variation in their values is due to different crystal structures of the specimens (Table 3).

Table 3

Binding energies (eV) of Mn 2p and Ca 2p electrons in calcium manganites

Sample	Mn		Ca	
	$2p_{3/2}$	$2p_{1/2}$	$2p_{3/2}$	$2p_{1/2}$
$CaMnO_3$	641.9	653.5	347.5	351.1
$CaMnO_3$[a]	640.8	652.2	347.3	351.0
$CaMn_2O_4$	641.8	653.4	347.5	351.0
$CaMn_2O_4$[b]	641.4	653.0	347.3	351.0
$CaMn_2O_4$[c]	641.7	653.3	347.4	351.1
MnO	640.6	652.2	–	–
Mn_3O_4	641.4	653.0	–	–
Mn_2O_3	641.9	653.5	–	–
MnO_2	642.2	653.8	–	–

[a] $CaMnO_3$ annealed in $N_2 + H_2$ (1:1) atmosphere at 1373 K for 3 h.

[b] $CaMn_2O_4$ annealed in $N_2 + H_2$ (1:1) atmosphere at 1373 K for 3 h (top portion).

[c] $CaMn_2O_4$ annealed in $N_2 + H_2$ (1:1) atmosphere at 1373 K for 3 h (cracked bottom portion).

Fig. 1.5.4 shows the temperature dependence of electrical resistivity, q versus T, for undoped and doped CaMnO3. It is evident that doping with either Y^{3+} or Bi^{3+} causes a decrease in the resistivity of CaMnO3. The doped specimens exhibit metal to insulator transition at around 160 K.

The resistivity of manganites depends on several factors including the valence states ofMn and oxygen

non-stoichiometry. Double exchange mechanism which involves hopping of electrons from Mn^{3+} ($t^3_{2g}e_g$) onto Mn^{4+} ($t^3\ _{2g}$) is usually invoked to explain variations in resistivity. The doping of CaMnO3 at Ca sites with trivalent Y^{3+} or Bi^{3+} ions introduces electrons by way of charge compensation leading to the formation Mn^{3+} in the matrix such that it is represented as

$Ca_{1-x}Y(Bi)_xMn^{4+}_{1-x}\ Mn_x^{3+}O_3$. Therefore the resistivities of the doped materials are less. Further, it is observed that the resistivity of Bi^{3+} doped specimen is the lowest, which can be attributed to its
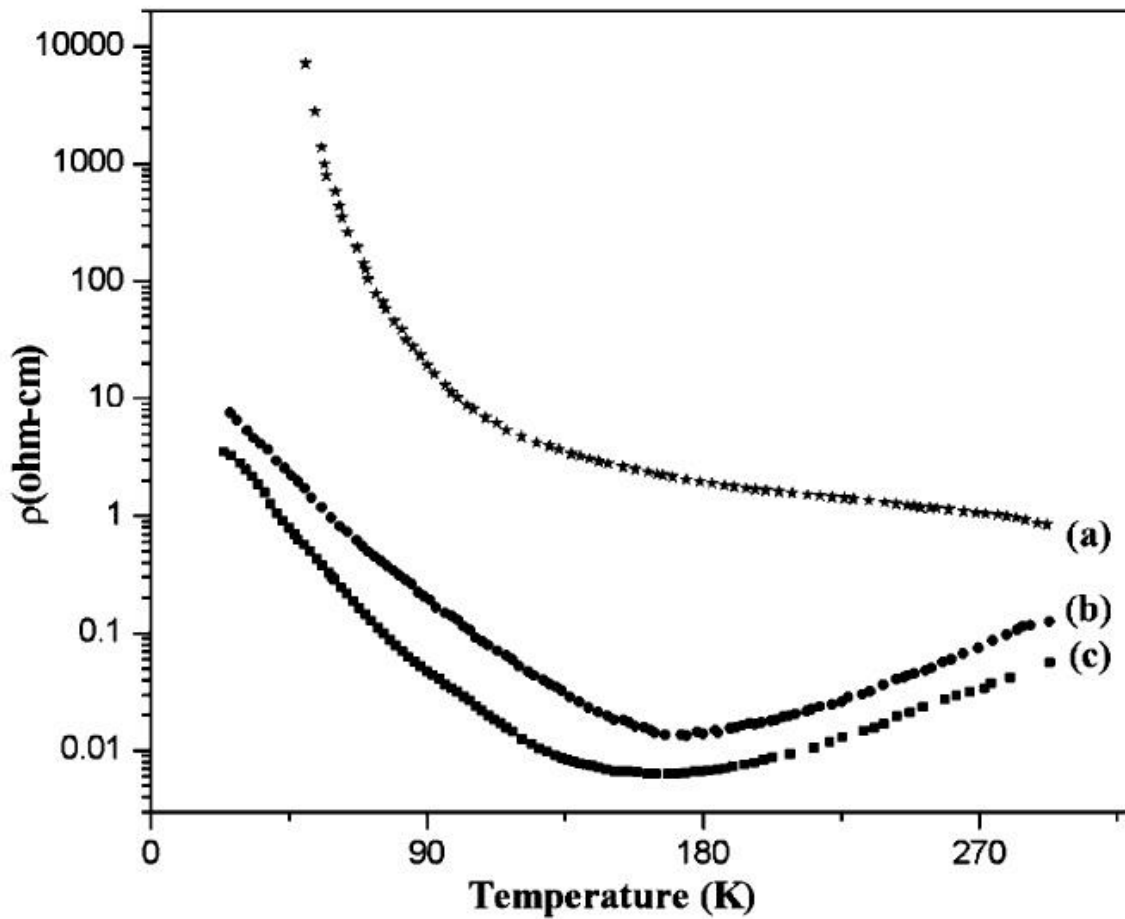
oxygen deficiency.

Figure 1.5.4: Resistivity versus temperature plot for (a) undoped,

3at% Y^{3+} and (c) 3at% Bi^{3+} doped CaMnO$_3$.

19

The removal of one oxygen ion (O^{2-}) results in the generation of two Mn^{3+} ions causing an increase in Mn(III) concentration and hence the increased conductivity of the material. However we could not explain the effect of Mn deficiency in the Y^{3+} doped specimen. The present study shows that dopants of similar charges may not introduce identical compositional changes. Resistivity measurements could not be performed on reduced specimens in view of the presence of micro cracks. However previous reports suggest that the resistivity of reduced manganites, $CaMnO_{3-\delta}$ is strongly influenced by oxygen deficiency, which controls the concentration of Mn^{3+} ions and, in turn the resistivity.

1.6 SUMMARY

3.05 MeV $^{16}O(\alpha,\alpha)^{16}O$ resonant scattering with enhanced sensitivity for oxygen provides the compositional analysis of calcium manganites with reasonably good accuracy. Doping in the Mn site of CaMnO3 with donors such as Y^{3+} or Bi^{3+} causes compositional changes in the material, which affect its electrical characteristics. However the phase identity of CaMnO3 (perovskite) is maintained on doping. Annealing of manganites in hydrogen atmosphere introduces significant structural and compositional changes that modify the modify the BS spectral features of the parent manganites. XPS measurements suggest the existence of Mn(II)/Mn(III) in the annealed specimens.

STRUCTURE OF PEROVSKITE

A perovskite is any material with the same type of crystal structure as calcium titanium oxide (CaTiO3), known as the perovskite structure, or $^{XII}A^{2+VI}B^{4}+X^{2-}{}_{3}$ with the oxygen in the face centers.

2.1 OVERVIEW

Perovskites take their name from the mineral, which was first discovered in the Ural mountains of Russia by Gustav Rose in 1839 and is named after Russian mineralogist L. A. Perovski (1792–1856). The general chemical formula for perovskite compounds is ABX3, where 'A' and 'B' are two cations of very different sizes, and X is an anion that bonds to both. The 'A' atoms are larger than the 'B' atoms.

The ideal cubic-symmetry structure has the B cation in 6-fold coordination, surrounded by an octahedron of anions, and the A cation in 12-fold cuboctahedral coordination. The relative ion size requirements for stability of the cubic structure are quite stringent, so slight buckling and distortion can produce several lower-symmetry distorted versions, in which the coordination numbers of A cations, B cations or both are reduced.

Natural compounds with this structure are perovskite, loparite, and the silicate perovskite bridgmanite.

2.2 STRUCTURE

The perovskite structure is adopted by many oxides that have the chemical formula ABO3. In the idealized cubic unit cell of such a compound, type 'A' atom sits at cube corner positions (0, 0, 0), type 'B' atom sits at body centre position (1/2, 1/2, 1/2) and oxygen atoms sit at face centred positions (1/2, 1/2, 0). (The diagram shows edges for an equivalent unit cell with A in body centre, B at the corners, and O in mid-edge).

The relative ion size requirements for stability of the cubic structure are quite stringent, so slight buckling and distortion can produce several lower-symmetry distorted versions, in which the coordination numbers of A cations, B cations or both are reduced.

Tilting of the BO_6 octahedra reduces the coordination of an undersized A cation from 12 to as low as 8. Conversely, off-centering of an undersized B cation within its octahedron allows it to attain a stable bonding pattern. The resulting electric dipole is responsible for the property of ferroelectricity and shown by perovskites such as BaTiO3 that distort in this fashion.

The orthorhombic and tetragonal phases are most common non-cubic variants. Complex perovskite structures contain two different B-site cations. This results in the possibility of ordered and disordered variants.

2.3 COMMON OCCURRENCE

The most common mineral in the Earth is bridgmanite, a magnesium-rich silicate which adopts the perovskite structure at high pressure. As pressure increases, the SiO44− tetrahedral units in the dominant silica-bearing minerals become unstable compared with SiO68− octahedral units.

At the pressure and temperature conditions of the lower mantle, the most abundant material is a perovskite-structured mineral with the formula $(Mg,Fe)SiO_3$, with the second most abundant material likely the rocksalt-structured $(Mg,Fe)O$ oxide, periclase.

At the high pressure conditions of the Earth's lower mantle, the pyroxene enstatite, $MgSiO_3$, transforms into a denser perovskite-structured polymorph; this phase may be the most common mineral in the Earth. This phase has the orthorhombically distorted perovskite structure ($GdFeO_3$-type structure) that is stable at pressures from ~24 GPa to ~110 GPa.

However, it cannot be transported from depths of several hundred km to the Earth's surface without transforming back into less dense materials. At higher pressures, $MgSiO_3$ perovskite transforms to post-perovskite.

Although the most common perovskite compounds contain oxygen, there are a few perovskite compounds that form without oxygen. Fluoride perovskites such as $NaMgF_3$ are well known. A large family of metallic perovskite compounds can be represented by RT_3M (R: rare-earth or other relatively large ion, T: transition metal ion and M: light metalloids).

The metalloids occupy the octahedrally coordinated "B" sites in these compounds. RPd_3B, RRh_3B and $CeRu_3C$ are examples. $MgCNi_3$ is a metallic perovskite compound and has received lot of attention because of its superconducting properties. An even more exotic type of perovskite is represented by the mixed oxide-aurides of Cs and Rb, such as Cs_3AuO, which contain large alkali cations in the traditional "anion" sites, bonded to O^{2-} and Au^- anions.

2.4 MATERIAL PROPERTIES

Perovskite materials exhibit many interesting and intriguing properties from both the theoretical and the application point of view. Colossal magnetoresistance, ferroelectricity, superconductivity,

charge ordering, spin dependent transport, high thermopower and the interplay of structural, magnetic and transport properties are commonly observed features in this family.

These compounds are used as sensors and catalyst electrodes in certain types of fuel cells and are candidates for memory devices and spintronics applications.

Many superconducting ceramic materials (the high temperature superconductors) have perovskite-like structures, often with 3 or more metals including copper, and some oxygen positions left vacant. One prime example is yttrium barium copper oxide which can be insulating or superconducting depending on the oxygen content.

Chemical engineers are considering a cobalt-based perovskite material as a replacement for platinum in catalytic converters in diesel vehicles.

2.5 APPLICATIONS

Physical properties of interest to materials science among perovskites include superconductivity, magnetoresistance, ionic conductivity, and a multitude of dielectric properties, which are of great importance in microelectronics and telecommunication.

Because of the flexibility of bond angles inherent in the perovskite structure there are many different types of distortions which can occur from the ideal structure. These include tilting of the octahedra, displacements of the cations out of the centers of their coordination polyhedra, and distortions of the octahedra driven by electronic factors (Jahn-Teller distortions).

2.6 PHOTOVOLTAICS

Synthetic perovskites have been identified as possible inexpensive base materials for high-efficiency commercial photovoltaics – they showed a conversion efficiency of up to 15% and can be manufactured using the same thin-film manufacturing techniques as that used for thin film silicon solar cells.

Methylammonium tin halides and methylammonium lead halides are of interest for use in dye-sensitized solar cells. In 2016, power conversion efficiency have reached 21%.[citation needed] In July 2016, a team of researchers led by Dr. Alexander Weber-Bargioni demonstrated that perovskite PV cells could reach a theoretical peak efficiency of 31%.

Among the methylammonium halides studied so far the most common is the methylammonium lead triiodide ($CH_3NH_3PbI_3$). It has a high charge carrier mobility and charge carrier lifetime that allow light-generated electrons and holes to move far enough to be extracted as current, instead of losing their energy as heat within the cell. $CH_3NH_3PbI_3$ effective diffusion lengths are some 100 nm for both electrons and holes.

Methylammonium halides are deposited by low-temperature solution methods (typically spin-coating). Other low-temperature (below 100 °C) solution-processed films tend to have considerably smaller diffusion lengths. Stranks et al. described nanostructured cells using a mixed methylammonium lead halide ($CH_3NH_3PbI_3-xCl_x$) and demonstrated one amorphous thin-film solar cell with an 11.4% conversion efficiency, and another that reached 15.4% using vacuum evaporation.

The film thickness of about 500 to 600 nm implies that the electron and hole diffusion lengths were at least of this order. They measured values of the diffusion length exceeding 1 μm for the mixed perovskite, an order of magnitude greater than the 100 nm for the pure iodide. They also showed that carrier lifetimes in the mixed perovskite are longer than in the pure iodide.

For $CH_3NH_3PbI_3$, open-circuit voltage (V_{OC}) typically approaches 1 V, while for $CH_3NH_3PbI(I,Cl)_3$ with low Cl content, $V_{OC} > 1.1$ V has been reported. Because the band gaps

(Eg) of both are 1.55 eV, VOC-to-Eg ratios are higher than usually observed for similar third-generation cells. With wider bandgap perovskites, VOC up to 1.3 V has been demonstrated.

The technique offers the potential of low cost because of the low temperature solution methods and the absence of rare elements. Cell durability is currently insufficient for commercial use.

Planar heterojunction perovskite solar cells can be manufactured in simplified device architectures (without complex nanostructures) using only vapor deposition. This technique produces 15% solar-to-electrical power conversion as measured under simulated full sunlight.

2.7 LIGHT EMITTING DIODES

Also in 2008 researchers demonstrated that perovskite can generate laser light. LaAlO3 doped with neodymium gave laser emission at 1080 nm. In 2014 it was shown that mixed methylammonium lead halide (CH3NH3PbI3-xClx) cells fashioned into optically pumped vertical-cavity surface-emitting lasers (VCSELs) convert visible pump light to near-IR laser light with a 70% efficiency.

2.8 LASERS

Due to their high photoluminesence quantum efficiencies, perovskites may be good candidates for use in light-emitting diodes (LEDs). However, the propensity for radiative recombination has mostly been observed at liquid nitrogen temperatures.

2.9 PHOTOELECTROLYSIS

In September 2014, researchers of EPFL in Lausanne, Switzerland reported achieving water electrolysis at 12.3% efficiency in a highly efficient and low-cost water-splitting cell using perovskite photovoltaics